16 November 2000

PHYSICS LETTERS B

Physics Letters B 493 (2000) 209–215

www.elsevier.nl/locate/npe

Structure of the weakly-bound nucleus ^{6}He studied via the ^{6}Li(t, ^{3}He)^{6}He reaction

T. Nakamura [a,b,*], T. Aumann [a,1], D. Bazin [a], Y. Blumenfeld [a,c], B.A. Brown [a,d], J. Caggiano [e], R. Clement [a,d], T. Glasmacher [a,d], P.A. Lofy [a,f], A. Navin [a,g], B.V. Pritychenko [a,d], B.M. Sherrill [a,d], J. Yurkon [a]

[a] *National Superconducting Cyclotron Laboratory, Michigan State University, East Lansing, MI 48824-1321, USA*
[b] *Department of Physics, Tokyo Institute of Technology, 2-12-1 O-Okayama, Meguro, Tokyo 152-8551, Japan*
[c] *Institut de Physique Nucleaire IN2P3-CNRS, 91406 Orsay, Cedex, France*
[d] *Department of Physics and Astronomy, Michigan State University, East Lansing, MI 48824, USA*
[e] *Physics Division, Argonne National Laboratory, Argonne IL 60439, USA*
[f] *Department of Chemistry, Michigan State University, East Lansing, MI 48824, USA*
[g] *Nuclear Physics Division, Bhabha Atomic Research Center, Trombay, Mumbai 400 085, India*

Received 27 June 2000; received in revised form 19 September 2000; accepted 19 September 2000
Editor: J.P. Schiffer

Abstract

The ^{6}Li(t, ^{3}He)^{6}He charge-exchange reaction leading to the weakly-bound nucleus ^{6}He has been studied at 336 MeV. Beyond the strong peaks for the known ground state ($J^\pi = 0^+$) and first excited state ($J^\pi = 2^+$, $E_x = 1.8$ MeV), a broad asymmetric structure around $E_x \sim 5$ MeV has been observed. The angular distribution of this structure exhibits the dominance of a $\Delta L = 1$ transition, indicating the existence of intruder states at low excitation energies in ^{6}He. © 2000 Elsevier Science B.V. All rights reserved.

PACS: 25.60.Lg; 21.10.Pc; 27.20.+n
Keywords: Halo/skin nucleus; Charge exchange reaction

Weakly-bound nuclei that are found in the vicinity of the drip lines have attracted much interest due to their exotic halo and skin structures [1,2]. One area that has not yet been well studied is the excited states in the continuum of these nuclei. These states may reflect the two-fold structure composed of a core and a surrounding cloud of very diffuse valence neutron(s). One related manifestation of halo structure is a substantially large E1 concentration at low excitation energies seen in the Coulomb dissociation [3–8]. Two-neutron halo nuclei, such as ^{6}He and ^{11}Li, are characterized by a three-body "Borromean" structure. A Borromean nucleus is a quantum three-body bound system (e.g., $\alpha + n + n$ in ^{6}He) where any of its two-body subsystems ($\alpha + n$ and $n + n$) is unbound. In these cases excitation of low-lying continuum structure, such as a soft-dipole excitation and a three-body 2^+ resonance, have been predicted by three-body theories [9–11].

* Corresponding author.
E-mail address: nakamura@ap.titech.ac.jp (T. Nakamura).
[1] Present address: Gesellschaft für Schwerionenforschung (GSI), Planckstr. 1, D-64291 Darmstadt, Germany.

0370-2693/00/$ – see front matter © 2000 Elsevier Science B.V. All rights reserved.
PII: S0370-2693(00)01146-1

It is interesting that low-lying intruder (non-normal parity) states play an important role in the structures of halo and skin nuclei. The one-neutron halo nucleus ^{11}Be contains an intruder $2s_{1/2}$ neutron configuration in its ground state where the $1p_{1/2}$ configuration is normally expected. The low-energy dipole excitation at $E_x \sim 1.3$ MeV was observed for ^{11}Li, indicating that the ground and/or excited states contain strong intruder configurations [12,13]. This phenomenon is associated with three effects [14]: (1) a reduction of the gap between the $1p$ and $1d2s$ shells from its value of 11.5 MeV in ^{16}O; (2) the increase in pairing energy when the intruder configurations involve open shells; and (3) the deformation energy of the intruder configuration associated with open-shell configuration. The combination of these effects results in situations where the configuration associated with excitations across the shell gap may become degenerate or lower in energy than the normal configuration.

In this work we have studied the structure of the weakly-bound nucleus ^{6}He by means of the charge-exchange reaction ^{6}Li$(t, {}^3$He$)^6$He. Since in the case of ^{6}He, reliable information on the core-n interaction exists, this nucleus serves as a prototype for understanding Borromean continuum structure. Furthermore, since the deformation of the ^{4}He core in ^{6}He is very small [15], the study of the intruder states may provide an exclusive measure for the effect of a reduction of a p–sd shell gap among the three possible effects for the low-lying intruder states.

In spite of this interest, the level structure of ^{6}He has not been well established except for the ground state ($J^\pi = 0^+$) and the first excited state ($E_x = 1.8$ MeV, $J^\pi = 2^+$). Beyond these states, three broad structures have been reported around 5 MeV, 15 MeV, and 23 MeV, although the observed levels appear to contain some inconsistencies [16]. The (n, p) reaction on ^{6}Li at intermediate energy is one of the useful tools to approach the structure of ^{6}He since simple distorted-wave theory is applicable. However, because the neutron beam is secondary, the (n, p) reaction suffers from low statistics and poor energy resolution, of the order of 1 MeV. Hence, it is difficult to resolve even the first excited state from the ground state of ^{6}He. Recently, the (^{7}Li, ^{7}Be) reaction as an alternative to (n, p) was used [17–19], where a low-lying structure at $E_x \sim 5$ MeV in ^{6}He was observed. However, there was some disagreement about the nature of this structure. Refs. [17,19] claimed that this structure occurs as a dipole excitation, while Ref. [18] assigned this structure to be a 2^+ state. One difficulty in using this reaction arises from the complicated reaction mechanism involved with the heavy-ion projectile ^{7}Li. For instance since this reaction is accompanied by an orbital angular momentum transfer for the projectile in addition to a target, the angular distribution is obtained by a superposition of many combinations of projectile and target angular momentum transfers [18]. On the other hand, the angular distribution for (n, p) is characterized by an orbital momentum transfer only for a target.

The $(t, {}^3$He$)$ reaction has recently been proven to be a powerful spectroscopic tool and possibly provides a better alternative to the (n, p) and (^{7}Li, ^{7}Be) reactions. At the National Superconducting Cyclotron Laboratory (NSCL), Michigan State University, $(t, {}^3$He$)$ reactions have been studied by using a secondary triton beam with a high resolution spectrograph (A1200 or S800) [20,21]. Using a dispersion matching technique, one can reach an energy resolution of a few hundred keV even though the secondary triton beam has a large momentum spread. The use of the S800 spectrograph with its wide angular acceptance ($\Delta\Omega = 20$ msr) enables us to obtain angular distribution with only a few angular settings, which compensates for the low intensity of the secondary beam. Furthermore, the mechanism of the $(t, {}^3$He$)$ reaction is analogous to (n, p), which facilitates the analysis of the reaction. For example, only $\Delta L = 0$ and $\Delta S = 0, 1$ are allowed for a projectile transition, the same as for (n, p). It is also important to note that similarities are seen between the (p, n) and the $({}^3$He$, t)$ reactions [22], the latter being mirror reaction of $(t, {}^3$He$)$.

The experiment was performed by using the S800 spectrograph at the NSCL. The secondary triton beam was produced from a ^{4}He beam of 140 MeV/u on a thick Be production target. The triton beam had a typical intensity of about 10^6 particles/s, a mean energy of 336 MeV with an energy spread of 1%. It was used to bombard a ^{6}Li target with a thickness of 17.4 mg/cm^2 (95% enriched). The ^{7}Li contaminants in the target hardly affect the spectrum. This is because up to $E_x = 7.7$ MeV in ^{6}He there is no contribution from the ^{7}Li$(t, {}^3$He$)$ ^{7}He reaction due to the very different reaction Q value. For higher excitations no significant contribution from ^{7}Li is expected due

to the small structureless charge-exchange strengths as shown in the ^{7}Li(n, p)^{7}He experiment [23]. The 1-mm-thick scintillator located 30.3 m upstream of the target was used to count each incoming beam particle and provided normalization for extracting cross sections.

The momentum of the outgoing ^{3}He ions were measured by the spectrograph operated in dispersion matching mode. Data were taken at three different angular settings centered at 0, 8 and 18 degrees. These settings covered the laboratory scattering angle, $\theta_{\rm lab}$, of about 0–5, 4–12, and 14–22 degrees, respectively. Positions and angles of the focal planes were measured by two cathode-readout drift chambers (CRDC) [24]. The ^{3}He particles were identified by the conventional $\Delta E - E$ method using the energy signals from three layers of plastic scintillators downstream of the CRDC's. The energy and scattering angle of each particle at the reaction was reconstructed from the CRDC information. The energy resolution was about 450 keV FWHM, which was mainly due to the energy loss difference between triton and ^{3}He ions in the target.

Data with a $(CH_2)_n$ target (18.4 mg/cm^2) were taken for calibration purposes. The kinematics lines ($\theta_{\rm lab}$ vs. Q) for the ^{12}C(t, ^{3}He)^{12}B(g.s.) and ^{1}H(t, ^{3}He)n reactions were used to verify that the angular reconstruction procedure was done correctly. This was also used to make a fine adjustment for the reconstruction procedure. The angular resolution was determined mainly by the incident triton beam divergence and was about 0.6 degrees FWHM. The normalization for the beam monitor scintillator was obtained using the known cross section of the ^{12}C(t, ^{3}He)^{12}B(g.s.) reaction at 0 degrees at 381 MeV (11.8 ± 1.4 mb/sr) [20]. The systematic uncertainty for the normalization was estimated to be about 20%, taking into consideration the uncertainty in the energy dependence of the cross section for ^{12}C(t, ^{3}He)^{12}B(g.s.) between 336 MeV and 381 MeV [20], and that in the secondary-beam transmission between the beam monitor and the target.

Fig. 1 shows the energy spectra obtained for the ^{6}Li(t, ^{3}He)^{6}He reaction at the 0°((a) and (b)) and 8°(c) settings of the S800. Besides the conspicuous peaks for the transitions to the ground and first excited states in ^{6}He, the spectra show the strong and broad structures at $E_{\rm x}$ ~5 MeV and ~15 MeV. The structure around 15 MeV persists at the higher angular setting, while the structure around 5 MeV rapidly decreases as $\theta_{\rm lab}$ increases. An interesting feature of the 5 MeV bump is its very asymmetric shape, as clearly seen in the figure.

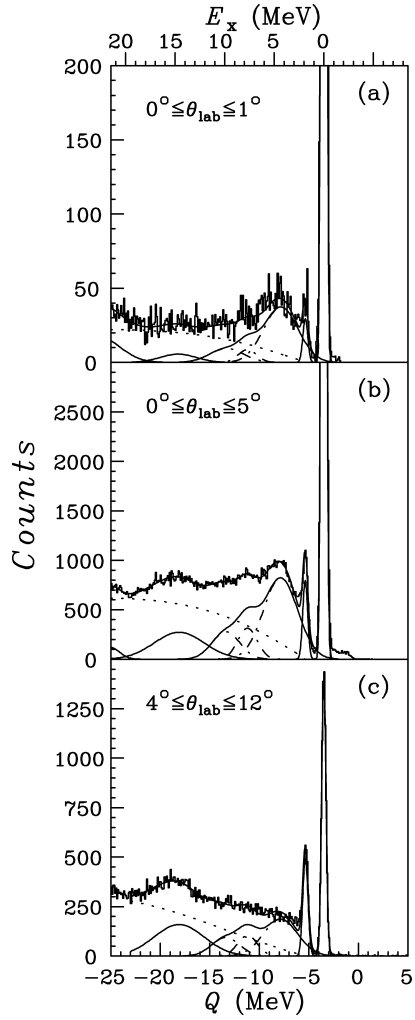

Fig. 1. Energy spectra for the ^{6}Li(t, ^{3}He)^{6}He reaction measured at 336 MeV for (a) 0°–1° in the laboratory scattering angle, (b) 0 degree setting of the S800 (0°–5°), and (c) 8 degree setting (4°–12°).

The spectral shape from the 0 degree setting (Fig. 1(b)) was analyzed by Gaussian peak-fitting. The asymmetric structure around 5 MeV was decomposed into three Gaussians to better study the nature of its components. This division is arbitrary, although at least three Gaussians are necessary to obtain an overall agreement of this structure, indicating its complex

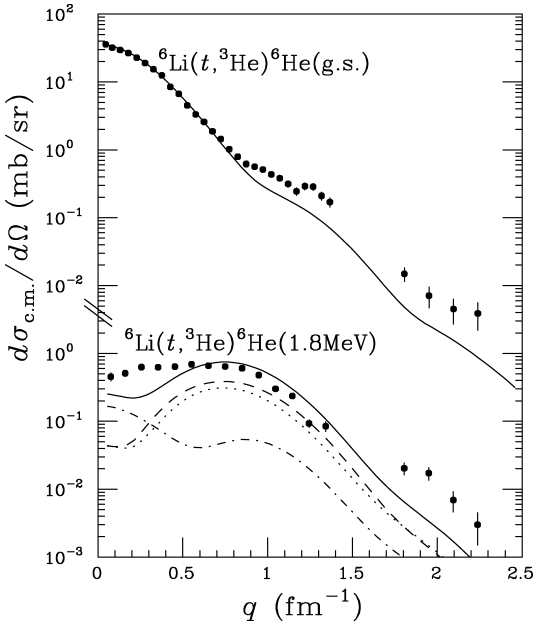

Fig. 2. Differential cross sections for the ^{6}Li(t, ^{3}He)^{6}He reaction leading to the ground state (upper) and first excited state (lower) in ^{6}He. The solid curves are the results of DWBA calculations with normalization of 1.0 and 0.8 for the ground and first excited state, respectively. For the transition to the first excited state, $\Delta J = 1, 2, 3$ components in the calculation are shown as dot-dashed, dotted, and dashed curves, respectively.

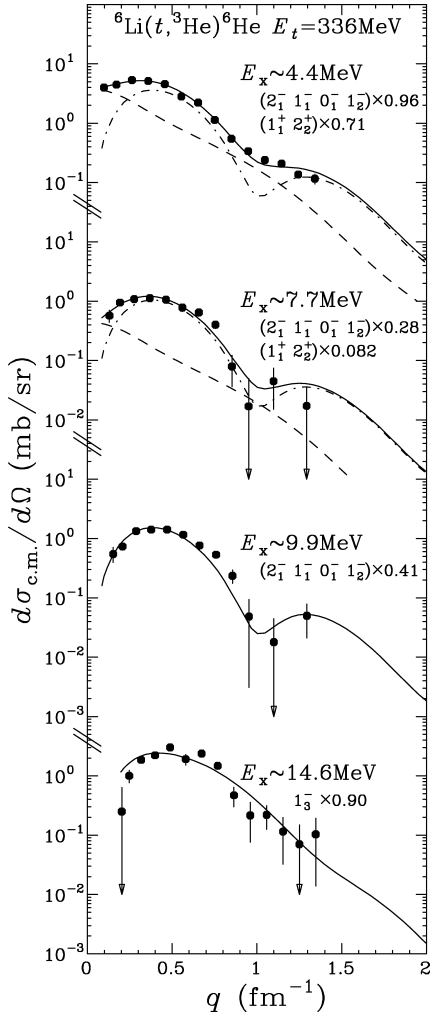

Fig. 3. Differential cross sections for the ^{6}Li(t, ^{3}He)^{6}He reaction leading to the 5 MeV (4.4, 7.7 and 9.9 MeV components) and 14.6 MeV structures. The results of a DWBA analysis are presented by the solid curves, normalized by the factor indicated for each state. For the 4.4 and 7.7 components in the 5 MeV structure, contributions from the non-normal parity states (2_1^-, 1_1^-, 0_1^-, 1_2^-) and normal parity states (2_2^+ 1_1^+) are shown by the dot-dashed and dashed curves, respectively.

composition. The best fit values for the locations of three Gaussians are 4.4 ± 0.1 MeV, 7.7 ± 0.2 MeV and 9.9 ± 0.4 MeV with Γ widths (FWHM) of 4.0 ± 0.1 MeV, 2.3 ± 0.4 MeV, and 3.3 ± 0.7 MeV, respectively. The structure around 15 MeV was best fitted with a location of 14.6 ± 0.2 MeV with a Γ width of 5.9 ± 0.7 MeV, consistent with results from the (n, p) [23] and (^{7}Li, ^{7}Be) reactions [18]. The continuum background (dotted curves in Fig. 1) was estimated with a semi-phenomenological parameterization of the quasi-free scattering [18]. With the same parameters for the locations and widths of these Gaussians, fits were also made for the spectra for (Figs. 1(a) and 1(c)). The differential cross sections shown below were obtained with the same procedure.

Differential cross sections as a function of momentum transfer q are shown in Fig. 2 for the ground and first excited states, and in Fig. 3 for the higher excited states. These angular distributions have a strong dependence on the orbital angular momentum transfer ΔL. Distorted Wave Born Approximation (DWBA) calculations were performed with the computer code DW81 [25]. In the DWBA, the transition amplitude is an integral of the product of distorted wave functions, a form factor that contains the effective projectile-nucleon interactions and transition density. Optical model parameters of a Woods–Saxon shape were ex-

Table 1
Optical-model potential parameters obtained from the analysis of our elastic scattering of ^{3}He on ^{6}Li at 335 MeV

V (MeV)	r (fm)	a (fm)	W (MeV)	r_I (fm)	a_I (fm)
−21.95	1.42	0.74	−7.62	1.49	0.57

tracted from our elastic scattering measurement of ^{3}He on ^{6}Li at 335 MeV at the 8 degree setting of the S800. The parameters obtained are shown in Table 1, and were used for the exit channel of the ^{6}Li$(t,{}^3$He$)^6$He reaction. The parameters for the entrance channel were determined by scaling the depths of the real and imaginary potentials by a factor of 0.85 [26].

The effective projectile-nucleon (t–N) interactions were based on the effective ^{3}He–N interactions derived phenomenologically for the (^{3}He$,t$) reactions [26,27]. The effective interactions V_{eff} in terms of single Yukawa potentials ($Y(r)$) were taken to be of the form

$$V_{\text{eff}}(r) = \left\{V_\tau Y(r/R_\tau) + V_{\sigma\tau} Y(r/R_{\sigma\tau})(\sigma_1 \cdot \sigma_2) + V_{T\tau} r^2 Y(r/R_{T\tau}) S_{12}\right\}(\tau_1 \cdot \tau_2), \quad (1)$$

where $V_\tau = 2.0$ MeV, $R_\tau = 1.415$ fm, $V_{\sigma\tau} = -3.0$ MeV, $R_{\sigma\tau} = 1.415$ fm, $V_{T\tau} = -3.0$ MeV fm^{-2}, and $R_{T\tau} = 0.878$ fm. Here, S_{12} denotes the usual tensor operator.

The wave functions and one-body transition densities for the input for DW81 were calculated with the shell-model computer code OXBASH [28]. We assumed harmonic-oscillator (HO) radial wave functions [29]. The positive (normal) parity states were calculated in the $1p$ shell basis with the CKHE interaction [30]. This interaction starts with the CKI two-body matrix elements of Cohen–Kurath [31], but the $T = 1$ two-body matrix elements were replaced by those obtained from a fit to the known binding energies and excitation energies of the He isotopes [30]. This modification of the $T = 1$ matrix elements reflects the influence of the neutron halo/skin nature of the neutron-rich He isotopes. The B(GT) value for the β decay of ^{6}He obtained with the CKHE wave functions is 5.53 compared to the experimental value of of 4.73 [18,32]. The small reduction of the experimental strength is typical of the quenching obtained for B(GT) values in the p-shell [32]. The B(GT) values

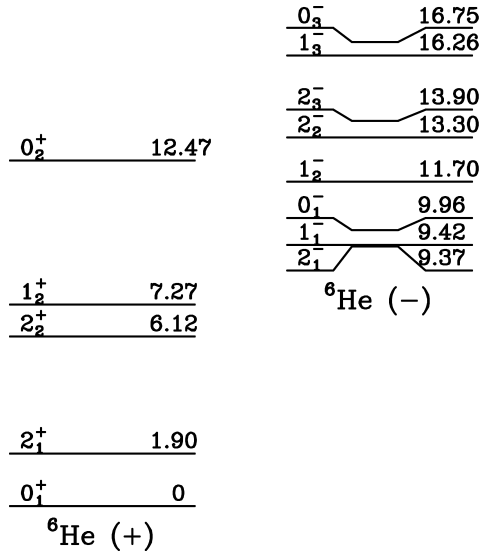

Fig. 4. Energy level scheme for positive (left) and negative (right) parity states of ^{6}He predicted by the shell model calculation.

calculated for the ^{6}Li to ^{6}He transitions are given in Table 3 of Ref. [18].

For the negative (non-normal) parity states we use the s–p–sd–pf model space with the WBT interaction of Warburton and Brown [33]. The configurations assumed for these non-normal parity states involve the excitation of one nucleon from the $1s$ shell to the $1p$ shell or one nucleon from the $1p$ shell to the $1d2s$ shell. This interaction was designed to describe non-normal parity states in the mass region $A = 10$–20. Its use here for $A = 6$ is outside of its intended range, and we do not expect the energies to be very realistic. However, the basic structure of the transition densities involving the excitation from the $1p$ shell ground state of ^{6}Li should be appropriate for an analysis of the reaction cross sections obtained in this experiment. The ^{6}He energy levels calculated from the CKHE (positive parity) and WBT (negative parity) interactions are summarized in Fig. 4.

Comparisons of the DWBA calculation with the experimental angular distributions for the ground and first excited states are shown in Fig. 2. The transition to the ground state (^{6}Li$(1^+) \rightarrow {}^6$He(0^+)) has a forward-peaked distribution, typical of a Gamow–Teller transition, while the transition to the first excited state (^{6}Li$(1^+) \rightarrow {}^6$He(2^+)) has a much broader shape, indicating a large mixture of a $\Delta L = 2$ transition. The

distribution for the ground state transition is in good agreement with the DWBA calculation (solid curve), in particular for the forward angles up to $q \sim 1.5\ \mathrm{fm}^{-1}$. The normalization factor here is 1.0. The harmonic oscillator size parameter b had to be adjusted to a larger value ($b = 2.57$ fm), which may be related to the large radius of the loosely-bound valence neutron of ^{6}He.

For the first excited state, reasonable agreement with the DWBA calculation is obtained with the same HO parameters as for the ground state. The shape is characterized by a mixture of $\Delta J = 1$ (mainly $\Delta L = 0$) and $\Delta J = 2, 3$ (mainly $\Delta L = 2$), as expected. The normalization factor for the calculated distribution is 0.8. The calculation underestimates the cross section at $q \sim 0$ which is dominated by the $\Delta L = 0$ component. We have found that the calculation for the $\Delta L = 0$ component is rather sensitive to the choice of the interactions in the shell model.

The angular distributions for the 5 MeV and 14.6 MeV structures are shown in Fig. 3. As described above, the 5 MeV bump was decomposed into three Gaussians that peak at 4.4 MeV, 7.7 MeV and 9.9 MeV. The angular distributions for these three Gaussians are broader than that of the ground state with $\Delta L = 0$, and narrower than that of the first excited state with $\Delta L = 2$ dominant. This fact suggests that the transition to the 5 MeV structure has $\Delta L = 1$ characteristics, indicating the existence of low-lying dipole states in ^{6}He. On the other hand, the cross section at $q \sim 0$ for the 4.4 MeV region is larger than for the 7.7 MeV and 9.9 MeV regions, suggesting that the structure has a $\Delta L = 0$ component at the lower excitation energies. Indeed, the DWBA calculation shows that the best agreement is obtained with an admixture of transitions to a negative parity states ($\Delta L = 1$), with those to the positive parity states ($\Delta L = 0, 2$) being only at lower excitations energies. In our shell model calculation we adopted first four negative parity states (2_1^-, 1_1^-, 0_1^-, 1_2^- in Fig. 4) for the $\Delta L = 1$ transition. These transitions were used since these levels are closely located, and their angular distributions are of similar shapes. For $\Delta L = 0, 2$ transition, we adopted two closely-located positive parity states (2_2^+ 1_1^+) shown in Fig. 4. It should be noted that the three-body calculation [9] also predicted the 2^+ state at about $E_x \sim 4$ MeV. Evidence for this 2^+ state was also seen in a recent ^{6}He+C experiment [34].

The angular distribution for the 14.6 MeV structure is shown on the bottom part of Fig. 3. The distribution is broader than those for the 5 MeV structure. The distribution is well reproduced assuming that the transition occurs to the predicted negative parity states at $E_x \sim 16$–20 MeV (Fig. 4). In Fig. 3 the calculation for the 1_3^- state is shown by the solid curve, which is in good agreement with the data. The assignment of the $\Delta L = 1$ transition is consistent with the result for the (n, p) reaction [23].

The difference between the $\Delta L = 1$ transitions to the 5 MeV and 14.6 MeV structures is that the former is dominated by a transition to $2s1p^{-1}$ (proton hole in the $1p$ orbital and neutron in $2s$ orbital in ^{6}Li), while the latter is dominated by the transition to $1p1s^{-1}$ and $1d1p^{-1}$ configurations. Since the $2s$ orbital has a larger mean radius than the $1s$ orbital, the angular distribution (in q space) is narrower for the 5 MeV structure. This result indicates that the gap between the $1p$ and $2s$ orbitals is about 5 MeV, significantly smaller than the $1s$–$1p$ and $1p$–$1d$ gaps of about 15 MeV.

To summarize, we have measured ^{6}Li$(t, {}^3$He$)^6$He reaction at 336 MeV. We have observed a broad asymmetric structure at $E_x \sim 5$ MeV and another structure at 14.6 MeV above the strong peaks for the ground and first excited states in ^{6}He. The angular distributions show that the structure around 5 MeV is dominated by the dipole states with a mixture of positive parity states in its lower-energy portion. The existence of intruder dipole states at such low energies suggests a quenching of the $1p$–$2s$ gap in this nucleus. The 14.6 MeV structure has been found to have a $\Delta L = 1$ shape, corresponding to the transition composed mainly of $1p1s^{-1}$ and $1d1p^{-1}$ components.

Acknowledgements

The authors wish to thank the operations staff at the NSCL for the production and tuning of the beam. We acknowledge S. Van der Werf, R. Anantaraman, S.M. Austin, A. Galonsky and J. Jänecke for invaluable discussions. We are also grateful to I.J. Thompson and B.V. Danilin for directing our interest to this problem.

This work is supported in part by the National Science Foundation under Contract Nos. PHY-9528844 and PHY-9605207.

References

[1] P.G. Hansen, A.S. Jensen, B. Jonson, Annu. Rev. Nucl. Sci. 45 (1995) 591, and references therein.
[2] I. Tanihata, Prog. Part. Nucl. Phys. 35 (1995) 505, and references therein.
[3] K. Ieki et al., Phys. Rev. Lett. 70 (1993) 730;
D. Sackett et al., Phys. Rev. C 48 (1993) 118.
[4] T. Nakamura et al., Phys. Lett. B 331 (1994) 296.
[5] S. Shimoura et al., Phys. Lett. B 348 (1995) 29.
[6] M. Zinser et al., Nucl. Phys. A 619 (1997) 151.
[7] T. Nakamura et al., Phys. Rev. Lett. 83 (1999) 1112.
[8] T. Aumann et al., Phys. Rev. C 59 (1999) 1252.
[9] B.V. Danilin et al., Phys. Rev. C 55 (1997) R577;
B.V. Danilin, I.J. Thompson, J.S. Vaagen, M.V. Zhukov, Nucl. Phys. A 632 (1998) 383.
[10] S.N. Ershov et al., Phys. Rev. C 56 (1997) 1483.
[11] A. Cobis, D.V. Fedorov, A.S. Jensen, Phys. Rev. Lett. 79 (1997) 2411.
[12] A.A. Korsheninnikov et al., Phys. Rev. Lett. 78 (1997) 2317.
[13] H. Simon et al., Phys. Rev. Lett. 83 (1999) 496.
[14] H. Esbensen, B.A. Brown, H. Sagawa, Phys. Rev. C 51 (1995) 1274.
[15] I. Tanihata et al., Phys. Lett. B 261 (1992) 261.
[16] F. Ajzenberg-Selove, Nucl. Phys. A 490 (1988) 1;
D.R. Tilley et al., Nucl. Phys., and references therein (in press).
[17] S.B. Sakuta et al., Europhys. Lett. 22 (7) (1993) 511.
[18] J. Jänecke et al., Phys. Rev. C 54 (1996) 1070.
[19] S. Nakayama et al., Phys. Rev. Lett. 85 (2000) 262.
[20] I. Daito et al., Phys. Lett. B 418 (1998) 27.
[21] B.M. Sherrill et al., Nucl. Instrum. Methods A 432 (1999) 299.
[22] I. Bergqvist et al., Nucl. Phys. A 469 (1987) 648.
[23] F. Brady et al., Phys. Rev. Lett. 51 (1983) 1320.
[24] J. Yurkon et al., Nucl. Instrum. Methods A 422 (1999) 291.
[25] R. Schaeffer, J. Raynal, DWBA70 code, extended version, J. Comfort.
[26] S. Van der Werf et al., Nucl. Phys. A 496 (1989) 305.
[27] S. Van der Werf, private communication.
[28] B.A. Brown, A. Etchegoyen, W.D.M. Rae, N.S. Godwin, Computer code OXBASH, 1984 (unpublished).
[29] J. Mildenberger et al., Phys. Rev. C 42 (1990) 732.
[30] J. Stevenson et al., Phys. Rev. C 37 (1988) 2220.
[31] S. Cohen, D. Kurath, Nucl. Phys. 73 (1965) 1.
[32] W.-T. Chou, E.K. Warburton, B.A. Brown, Phys. Rev. C 47 (1993) 163.
[33] E.K. Warburton, B.A. Brown, Phys. Rev. C 46 (1992) 923.
[34] D. Aleksandrov et al., Nucl. Phys. A 669 (2000) 51.